ARMA 17-873

Effect of Injection Rate on Hydraulic Fracturing of Opalinus Clay Shale

Morgan, S.P., Li, B.Q. and Einstein, H.H.
Massachusetts Institute of Technology, Cambridge, MA, USA

ABSTRACT: For hydraulic fracturing operations in the field, the pumping rate is generally controlled but it is not fully understood how this affects the resulting fracture processes. This paper presents the results of an experimental study using a laboratory hydraulic fracturing setup, in which the injection rate was varied across four experiments, and the fracturing process was observed visually as well as with acoustic emission sensors. Prismatic 2 x 4 x 1 in. specimens of Opalinus clay shale, with a pre-cut 0.33 in. width flaw, were subjected to hydraulic pressure under constant biaxial far-field loading conditions. The pressure was measured internally inside the flaw as well as at the pressure volume actuator. Both a high speed- and a high resolution camera were used to visually record changes on the face of the specimen (i.e. fracturing). Acoustic emissions were recorded with an array of eight piezoceramic sensors embedded in specialized platens. The results of the experiments were then used in an analysis of the peak pressures and fracture propagation speed related to the injection rate. Higher peak pressures, fracturing speeds and fracturing accelerations were observed with higher injection rates. Additionally, the spectral analysis of the largest AE events showed that the highest injection rates resulted in higher power at lower frequencies. The highest injection rate was also associated with greater AE activity in general.

1. INTRODUCTION AND BACKGROUND

For hydraulic fracturing operations in the field, the pumping rate is generally controlled but it is not fully understood how this affects the resulting fracture processes. Recently, there has been an increase in the number of experimental studies being conducted on hydraulic fracturing in the laboratory. Experiments on natural rock typically use external displacement measurements, acoustic emission observation and post-failure inspection often combined with resin to capture the fracturing behavior during hydraulic fracture (Casas et al., 2006; Lecampion et al., 2015; Stanchitis et al., 2015a; Stanchitis et al., 2015b). Other researchers have used transparent model material, such as PMMA, to visualize the fractures (Rubin, 1984; Bunger et al., 2005; Lecampion et al., 2015). Visualizing the fractures in a natural rock, in real-time while applying confining pressures, has been difficult to achieve in the laboratory.

Additionally, many of these previous hydraulic fracturing studies have varied the rock (Benne et al., 2014; Stoeckhert et al., 2014; Cheng et al., 2015), confining stress and fluid viscosity (Barla et al., 1986; Ishida et al., 2004) while keeping a constant, controlled injection rate. The effect of injection rate on the breakdown pressure has also been investigated (Solberg et al., 1980; Zeng and Roegiers, 2002), while others studied the effect of pressurization rate (Haimson and Fairhurst, 1969; Zoback et al., 1977). However, capturing the fracture evolution during such tests can be very difficult as well.

2. EXPERIMENTAL PROCEDURE AND SETUP

2.1. Test Setup

The four hydraulic fracturing tests were conducted on prismatic Opalinus clay shale specimens with a single pre-cut flaw (Figure 1). The tests were done in a biaxial load frame with a transparent clamp seal on the front and back faces (Refer to Figure 1). In addition, high speed- and high resolution cameras were used to capture the fracturing processes, with 1,000 frames per second (fps) at 2 Megapixels (MP) and 0.5 fps at 20 MP, respectively. Eight acoustic emission sensors, spring loaded in specialized loading platens, were used to monitor acoustic activity in the specimens. The flaw was pressured using a 15 MPa capacity pressure volume actuator (PVA), and the pressures were recorded in the actuator as well as directly inside the flaw.

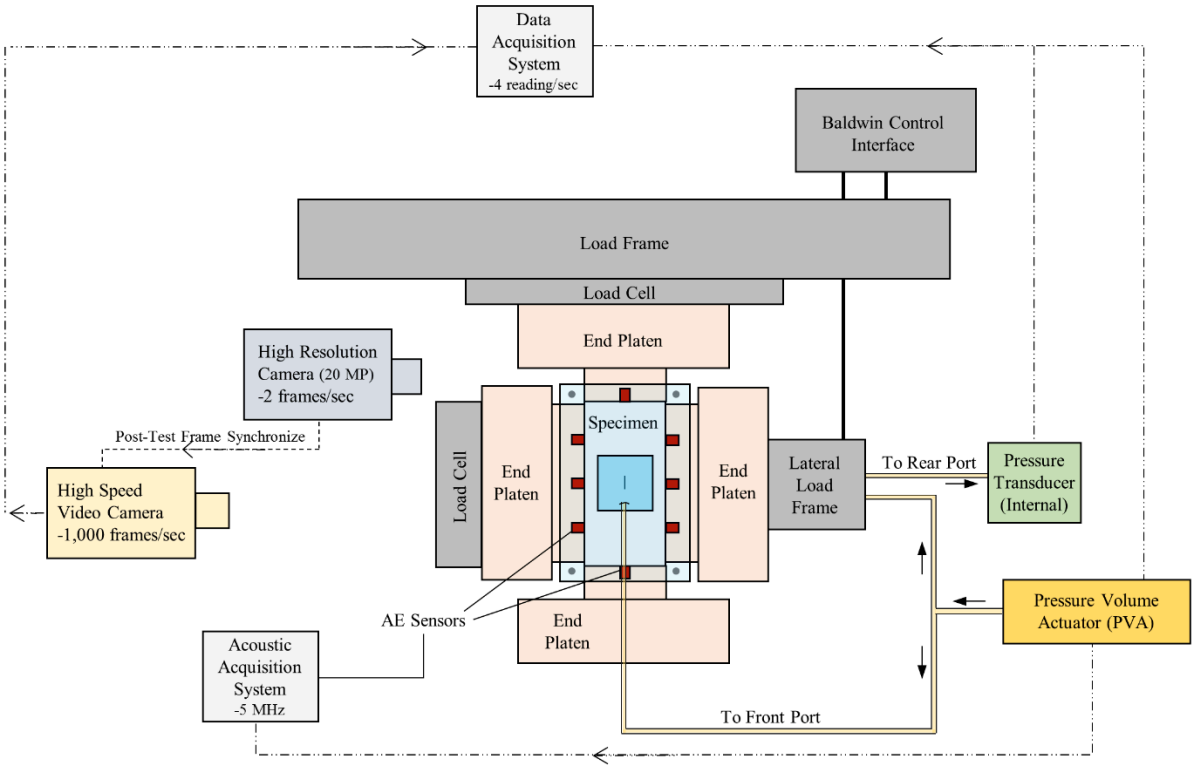

Figure 1 - Schematic of the experimental setup used in this study. The specimen was loaded to a constant axial and lateral load, and then fluid was injected into a pre-cut flaw. The fractures were observed using a high-speed camera, a high-resolution camera and an acoustic emission system. The fluid pressures were measured in the pressure volume actuator and internally in the flaw.

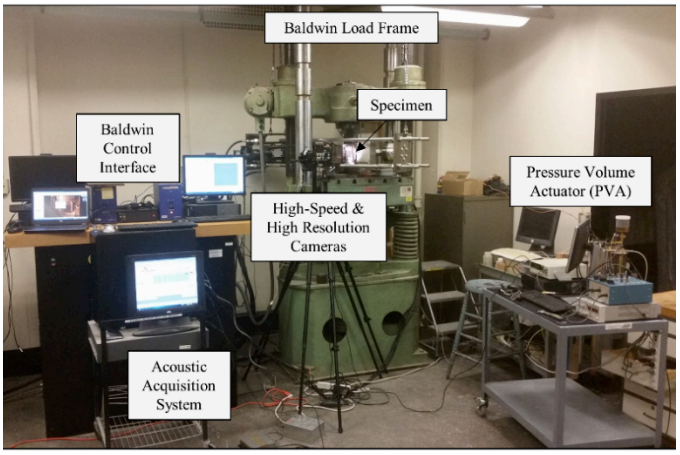

Figure 2 - Photo of the experimental setup used in this study.

The Opalinus clay shale specimens were dry cut from cores extracted from the Mont Terri Rock Laboratory in Switzerland [Refer to Morgan and Einstein (2014) for the cutting process]. The specimens were approximately 4 x 2 x1 in [101 x 50 x 25 mm] with a single vertical flaw of 0.33 x 0.035 in [8.5 x 0.9 mm] (Figure 3a). The naturally occurring bedding planes were oriented horizontally. The pressure-sealing device consisted of two 1.5 x 1.5 in [38 x 38 mm] polycarbonate seals, with an embedded silicon membrane, on the front and back faces of the specimen (Figure 3b and c). The 1.5 x 1.5 in polycarbonate seals were clamped to the specimen with a steel plate in the back and a thick polycarbonate plate the front via four bolts on the corners. Hydraulic oil (viscosity $\mu \approx 40$ cP) was injected into the flaw using two 0.025 in (0.64 mm) diameter tubes, one in the front and one in the back.

The testing process was performed in the following order:

1) Attached the seal and loading platens to the specimen
2) Placed the specimen into the loading frame and applied constant axial (4.5 MPa) and lateral (1 MPa) stress
3) The injection tubing was connected to the PVA and the seal was tightened
4) The flaw and plumbing lines were 'saturated' by injecting the fluid at a low injection rate with an open tube in the back
5) 'Saturation' was stopped and the 'internal' flaw pressure transducer was attached
6) Injection began at the prescribed injection rate
7) Once the specimen fractured, flow through the fracture occurred and the high-speed video was manually triggered.
8) The injection pump was stopped and the pressures dropped to a constant value

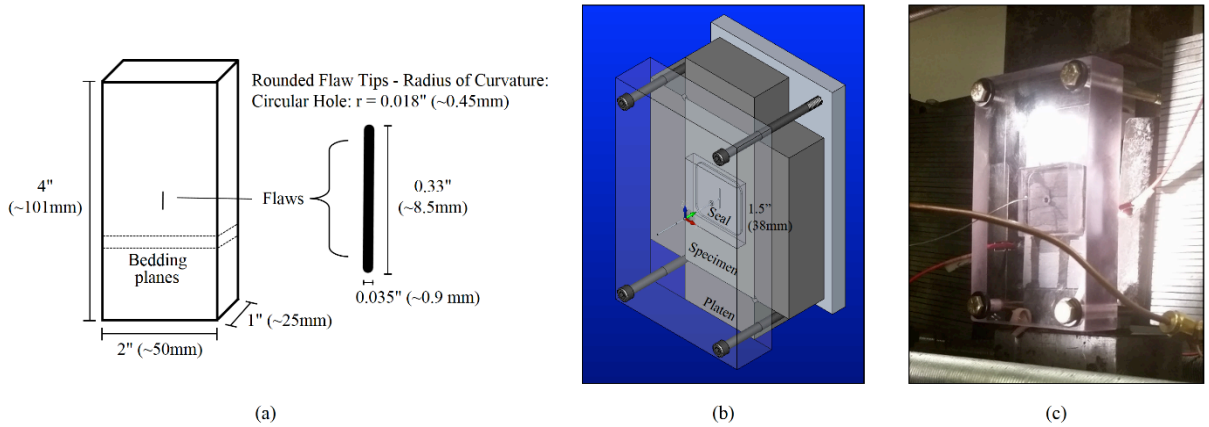

Figure 3 - Specimen and flaw pressurization device configuration. (a) Schematic of the specimen and pre-cut flaw dimensions, horizontal bedding planes. (b) Schematic of the flaw pressurization device with a 1.5 in [3.81 cm] square seal. (c) Photo of the flaw pressurization device.

2.2. *Acoustic Emissions Setup*

The experiment was instrumented with eight PAC (Physical Acoustics Corporation) Micro30S sensors, coupled with honey to the surface of the Opalinus clay shale. All sensors were connected to PCI-2 data acquisition cards from PAC at 5 MHz, with 45 dB trigger. The AE sensors were located as shown in Figure 4; placed into recesses in the loading platens and pressed against the shale with 10 kgf steel springs (Figure 4).

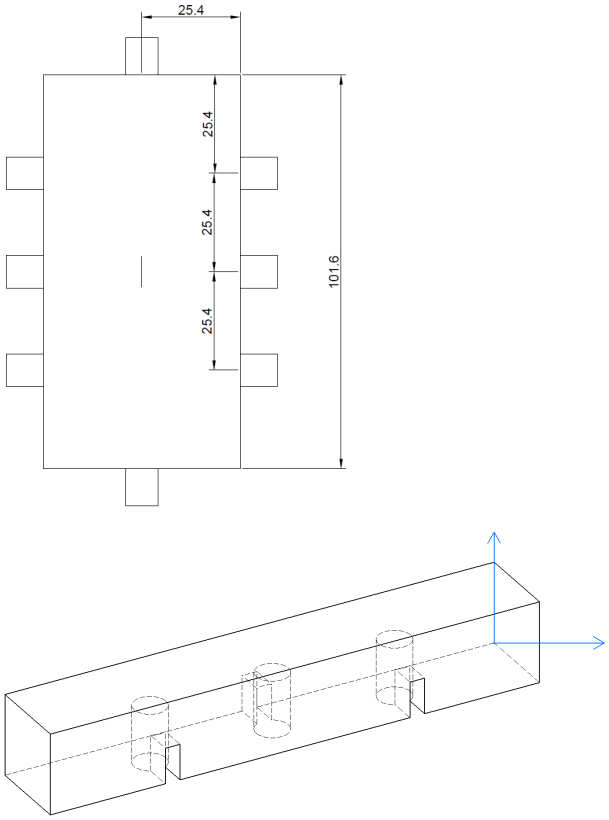

Figure 4 - (Top) AE sensor locations. (Bottom) Isometric view of sensor recesses within loading platens.

2.3. *Specimens Tested*

Four specimens were tested with different injection (flow) rates to investigate their effects on the fracturing behavior (Figure 5). The lateral and axial loads were held at a constant 4.5 MPa and 1 MPa, respectively. These stresses were chosen because they are below the fracture initiation stress for this flaw geometry observed in dry tests (without hydraulic fracture). The stresses were first applied isotropically to 1 MPa and then the axial load was increased to 4.5 MPa.

The four injection rates used were 0.0059 ml/s, 0.0188 mL/s, 0.0807 mL/s, and 0.3903 mL/s. The highest and lowest injection rates were defined by the physical limits of the PVA used in this experimental setup.

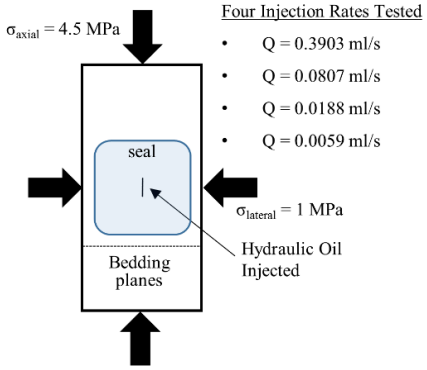

Figure 5 - Specimens tested in this study. Constant axial (4.5 MPa) and lateral (1 MPa) external stresses were applied. Hydraulic oil was injected at different rates. Four specimens were tested each with a different injection rate.

Note that given the set of injection rates and the fluid viscosity used in this study, the fracturing processes were likely in the toughness dominated regimes for all of the injection rates tested [as described by Bunger et al. (2005) and others]. An injection fluid with a much higher viscosity would be needed in order to achieve a viscosity dominated fracturing regime.

3. PRESSURE-FRACTURE RESULTS

3.1. Fracture Progression

Figure 6 shows the progression of fractures over time, and how they relate to the pressure in the flaw and in the PVA pump for the test with the 0.0807 mL/s injection rate. Fractures initiated at the flaw tips and then propagated diagonally toward the edge of the seal. Often, fractures propagated along natural horizontal bedding planes (See fracture B in Figure 6). A decline in the slope of the internal pressure versus time curve occurred at the first fracture initiation, and the internal pressure dropped when fractures reached the seal boundary.

The observed fracture patterns for the different injection rates tested are shown in Figure 7. At lower injection rates (Q=0.0059, 0.0188 mL/s) the fracturing consisted of simply two fractures initiating at the flaw tips and then propagating up and down towards the direction of maximum principal stress. These fractures were not perfectly straight, alternating between following the bedding planes and cutting across the layers between the bedding planes. At high injection rates (Q=0.0807, 0.3903 mL/s) more fractures occurred (>3 fractures) and their location and their patterns became more complex. This included longer fractures along bedding planes and fractures that branched.

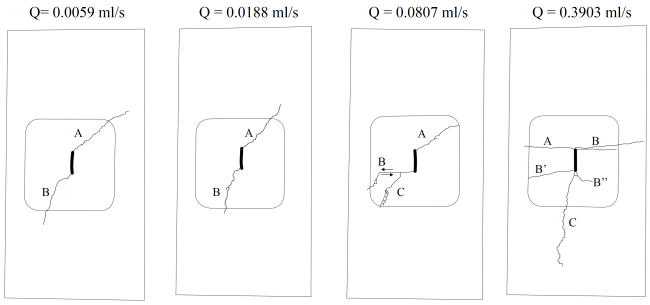

Figure 7 - Fracture patterns for different injection rates. The fractures are labeled alphabetically in chronological order. The fractures are usually tensile, however, some sliding was observed in fracture B of the specimen with Q = 0.0807 mL/s.

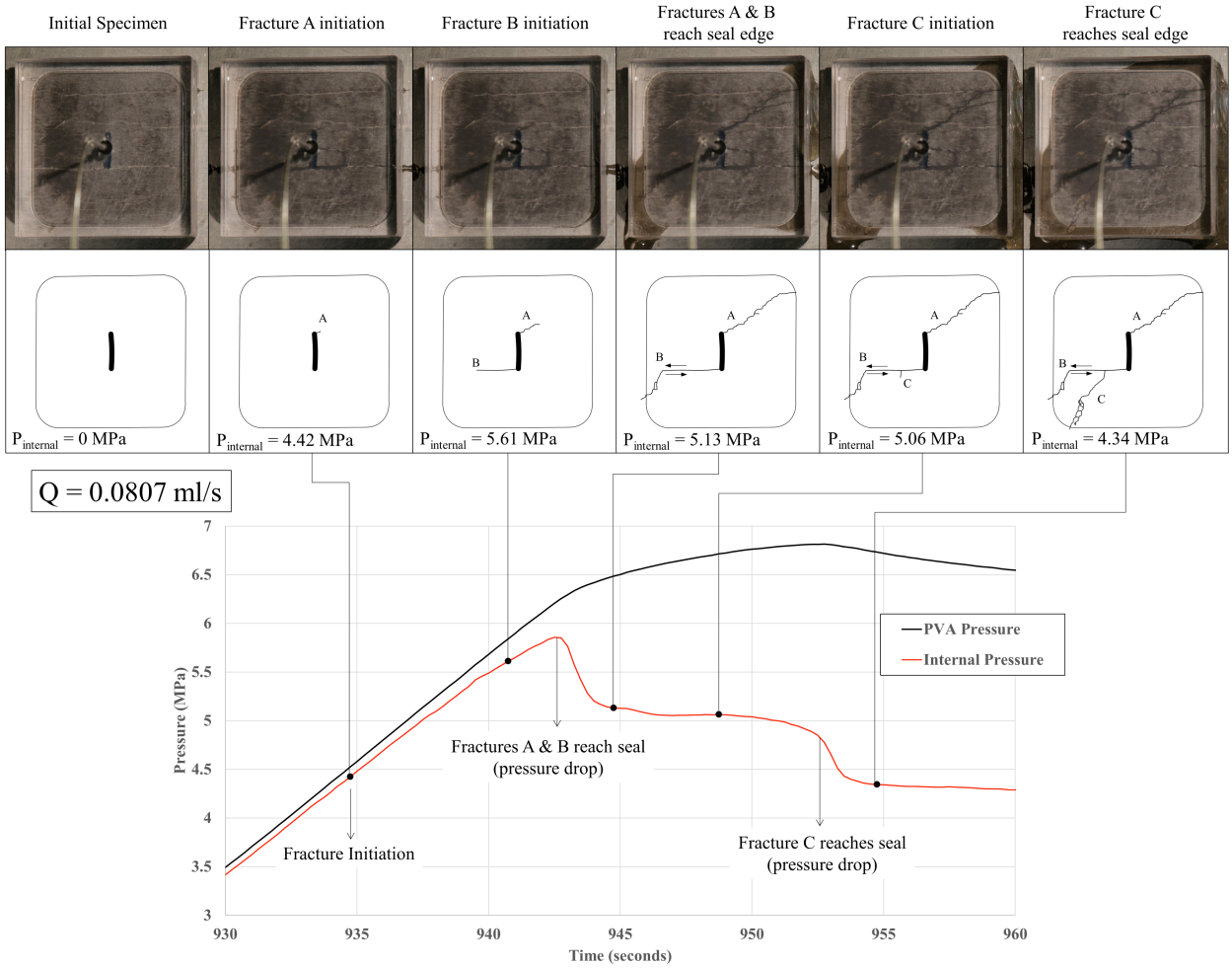

Figure 4 - Fracture progression and pressure-time curves for the test with 0.0807 mL/s injection rate. The PVA pressure was measured at the pump and the internal pressure was measured directly in the flaw. A decrease in the slope of the internal pressure versus time curve was observed at the first fracture initiation and a drop in the internal pressure were observed when fractures reached the seal boundary.

3.2. *Fracture Speed*

By using multiple images taken during the tests, and identifying the tip of each fracture as it propagated, the evolution of the fracture speed was determined for all fractures (Figure 8). In general, as the injection rate was increased the maximum fracture speed observed for the fractures also increased. Also, the specimens tested with higher injection rates showed higher fracturing accelerations (slopes in Figure 8).

It should be noted that there was some variability in the fracture speed, as expected when using a natural rock, such as a faster propagating fracture for the slowest injection rate or a slowly propagating fracture at the highest injection rate (Refer to Figure 8). However, the general trend between higher injection rate and higher fracture speed appeared to hold.

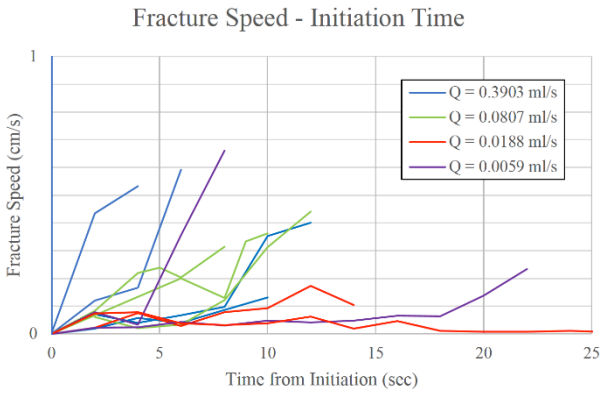

Figure 8 – Fracture speeds observed in this study. Speeds of the fractures are shown over time, starting at each fracture's initiation time. Specimens tested with higher injection rates showed higher fracture speeds and higher fracture acceleration (slope). The number of fractures for each injection rate was different (See Figure 7).

3.3. *Pressure-Time Results*

The effects of injection rate on the evolution of internal flaw pressure over time were also analyzed (Figure 9). This included fracture initiation, fractures propagating beyond the edge of the seal, and then constant pressure after the pump (injection) was stopped (Refer to Figure 9). As expected from previous studies, higher breakdown (maximum internal) pressures were observed for tests with higher injection rates.

Interestingly, the residual internal pressure, i.e. the equilibrated pressure after the pump was stopped, was close to 1 MPa for all tests. This was the same stress level as the lateral stress and therefore may be considered as the equivalent of the "fracture closure stress" observed in the field.

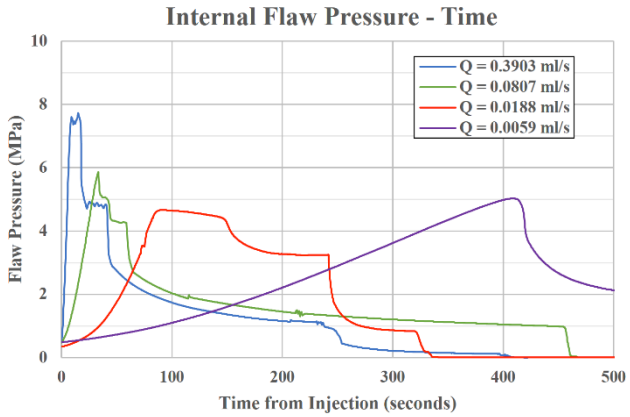

Figure 9 - Evolution of flaw pressure over time for the four injection rates tested measured with a transducer inside the pressurized flaw.

For each test, the internal flaw pressure when fractures initiated, the maximum internal pressure and the maximum PVA pump pressure were determined (Figure 10). Significant increases in the maximum PVA and internal flaw pressures were observed at higher injection rates. Additionally, large deviations between the PVA and internal flaw pressures were observed as the injection rate increased. The internal flaw pressure at fracture initiation was reasonably similar for all injection rates and was approximately the same as the applied axial stress (4.5 MPa).

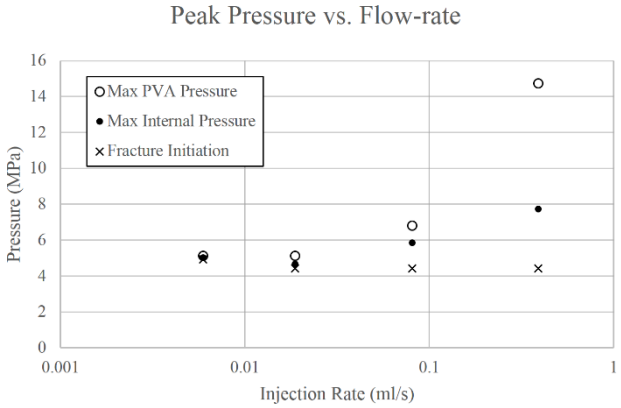

Figure 10 - Summary of the pressure results for the different injection rates. Increases in maximum pump (PVA)- and internal flaw pressures were observed at high injection rates. The fracture initiation pressure was approximately the same for all injection rates.

4. ACOUSTIC EMISSIONS (AE) RESULTS

4.1 AE Analysis Procedure

AE event locations were calculated with an error tolerance of 1 cm using an anisotropic velocity model with 3000 m/s along bedding and 2500 m/s perpendicular to bedding. Moment tensor decomposition was done assuming an isotropic material according to

the SiGMA framework as defined in Grosse and Ohtsu (2008).

4.2. AE Analysis Results

The AE equipment set-up was the same for all specimens; the number of events recorded varied significantly. Table 1 shows that the fastest injection rate produced the most AE events, followed by the slowest injection rate. The amplitudes appear to follow a similar trend.

Applying moment tensor decomposition, it appears that the double-couple (DC) contribution is dominant for three out of four injection rates. It was also observed that the isotropic component was greater than the compensated linear vector dipole (CLVD) component. In general, the DC component decreases while the CLVD and isotropic components increase with increasing injection rate.

Table 1 - Summary of AE data for all four injection rates.

	0.0059 mL/s	**0.0188 mL/s**	**0.0807 mL/s**	**0.3903 mL/s**
Number of detected events	5	1	2	25
Average DC (Shear)	0.6493	0.5715	0.092	0.5506
Average CLVD (Deviatoric)	0.1336	0.1632	0.3459	0.1712
Average ISO (Isotropic)	0.2171	0.2653	0.5621	0.2782
Max amplitude (dB)	75	69	76	80

The AE event locations for the fastest injection rate are shown in Figure 11. It appears that the events initially occur closer to the center of the specimen, and then move away from the flaw tips with time. It also appears that the events closest to the initial flaw are closer to a horizontal orientation, suggesting that microcracking occurred preferentially along the bedding of the Opalinus clay shale.

Figure 12 shows the spectra for the largest AE event for each injection rate. The spectrum for each injection rate is the mean over all channels for that event, where each channel's spectrum is calculated over an 800 µs window centered on the first arrival.

It appears that the fastest injection rate contains the highest power, particularly at lower frequencies, which indicates a larger fault area according to classic seismology theory, which states that the radius of a rupture is inversely proportional to its corner frequency (Shearer, 2009). However, this observation also appears to be true for the slowest injection rate, which also produced a larger number of AE events and contained an anomalously fast-growing fracture compared to the 0.01876 and 0.08065 mL/s experiments, as seen previously in section 3.2.

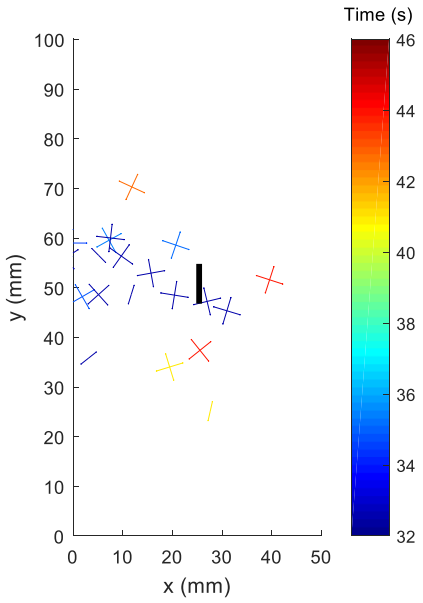

Figure 5 - AE event locations and orientations for the 0.39025 mL/s injection rate experiment. Crosses indicate conjugate shear planes for shear events; the single lines indicate opening direction of non-DC events. Thick black line is the flaw.

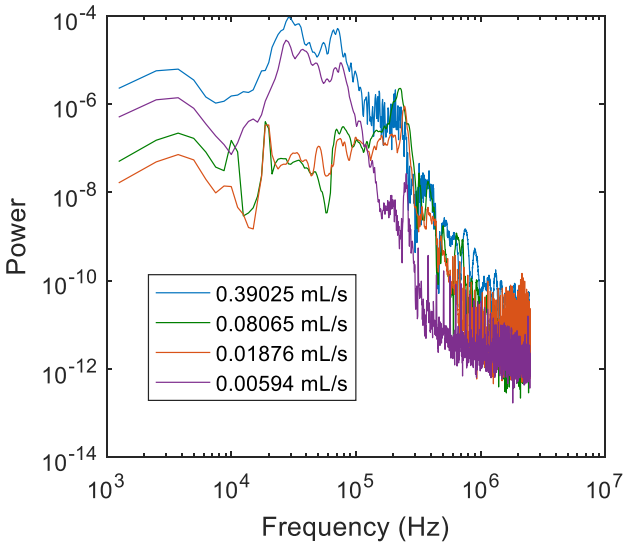

Figure 12 - Spectra for largest event seen at each injection rate.

4.3. Comparison of AE Data to Fracture Process

Figure 13 shows AE amplitude and pressure over time for the different injection rates. In three of the four cases, the high amplitude events corresponded to peak PVA pressure. As seen in the previous section, this point in time corresponds to significant fracture propagation resulting in the fracture reaching the seal boundaries, such that the pressure drops significantly. This also implies that, in general, fracture initiation does not produce significant AE activity in some cases.

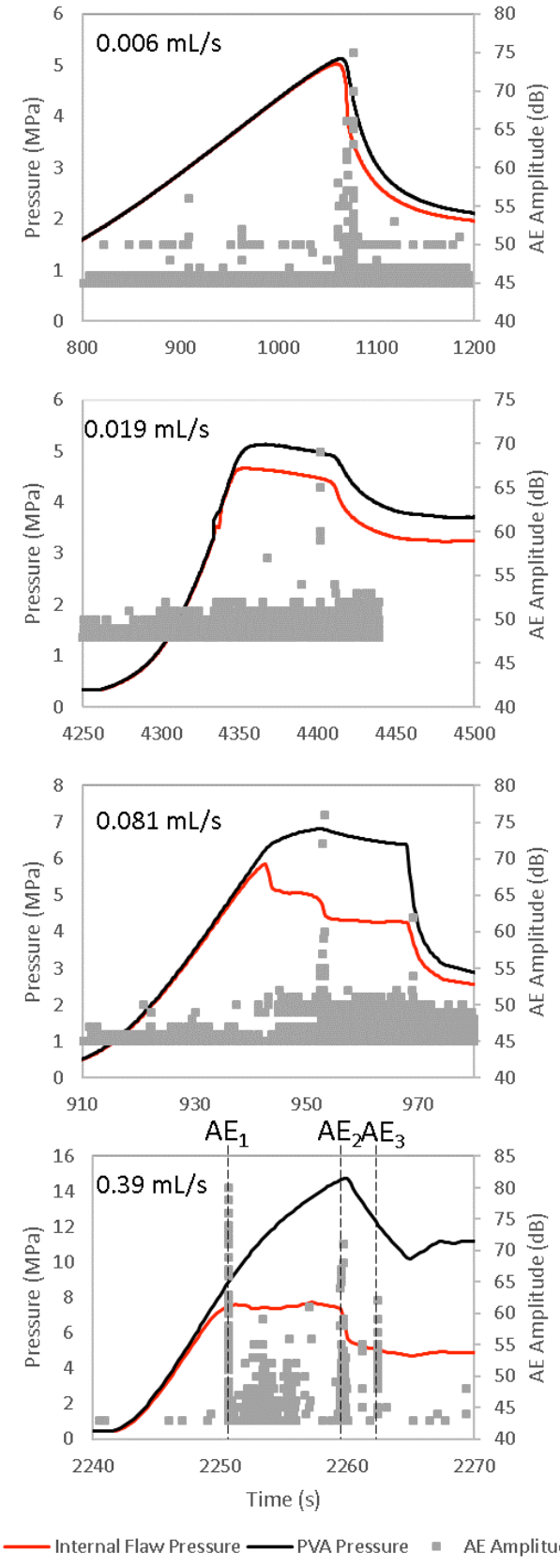

Figure 13 - Pressure and AE amplitude data for the four injection rate experiments.

The data were further analyzed for the fastest injection rate, where three main AE events (AE1, AE2, AE3) were detected. The first event corresponds to fracture initiation of fracture B shown in Figure 7, along with significant process zone development of fractures B' and B''. AE2 had a lower amplitude, and corresponds to the entire fracture initiation and propagation of fracture C. AE3 corresponds to continued propagation of existing fractures. It is interesting to note that AE1, which corresponds to a series of slower fractures, has more power at lower frequencies than AE2 (Figure 14), which is a fast fracture.

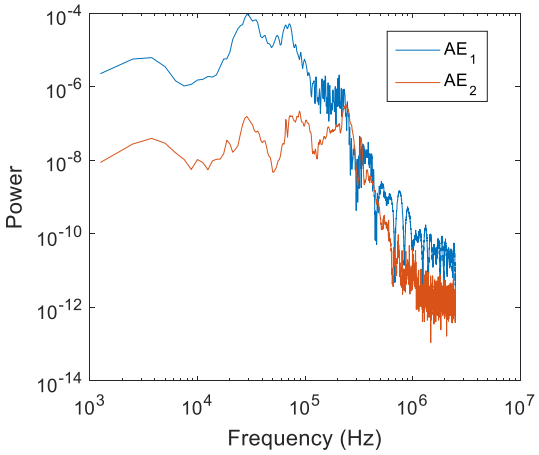

Figure 6 - Power spectra of AE1 and AE2 (Refer to **Error! Reference source not found.**).

5. DISCUSSION AND CONCLUSIONS

This study investigated the effect of four different injection rates on prismatic Opalinus clay shale specimens with a pre-cut vertical flaw and constant external biaxial stresses. Increasing the injection rate had a significant effect on the complexity and amount of fracturing that was observed. As a result, the fractures appeared less consistent and predictable, branching out in many directions as the injection rate increased. In a practical sense, this means that higher injection rates will increase the effective fracturing area, at the cost of predictable and more controlled fractures.

Additionally, increasing the injection rate showed an increase in the maximum internal pressure (typically referred to as breakdown pressure). Other studies on the injection rate, such as Solberg et al., 1980 observed a log-linear relationship between injection rate and breakdown pressure. However, Barla et al., 1986 observed a relatively constant breakdown pressure at low pressurization rates and an increase in breakdown pressure at higher rates, similar to the present study. Note, however, that Barla's experiments (pressure controlled) were run differently from the present study (injection rate controlled).

In terms of AE, it appears that the double couple (DC) component decreases as the injection rate increases, indicating a more expansive type of rupture with faster

injection. An analysis of the AE event orientations showed that initially the events appear to be oriented with bedding, but evolve to become oriented diagonally to bedding over time. When comparing AE to the fracturing process, it appears that breakdown produces AE activity, while fracture initiation only produced AE for the fastest injection rate. Overall, the highest injection rate produces a much more micro seismically active fracture process than the lower injection rates.

ACKNOWLEDGEMENTS

The authors would like to acknowledge the support of this research by TOTAL in the context of the project Multi-scale Shale Gas Collaboratory. We not only received financial support but also were helped through many constructive discussions with our technical contacts.

We would also like to thank Swisstopo and the Mt. Terri Laboratory (Dr. Ch. Nussbaum) for making the Opalinus shale cores available to us.

REFERENCES

1. Barla, G., P. Bertacchi, A. Zaninetti, P. P. Rossi and I. Vielmo (1986) Hydraulic fracturing testing method for rock stress measurements in Italy. *Proceedings of the International Symposium on Rock Stress and Rock Stress Measurements.* Stockholm. 332-340
2. Brenne, S., M. Molenda, F. Stöckhert and M. Alber, (2014) Hydraulic Fracturing of a Devonian Slate under confining pressure – with emphasis on cleavage inclination. *ISRM - Rock Engineering and Rock Mechanics: Structures in and on Rock Masses.* Taylor & Francis Group*,* London. 1369-1373.
3. Bunger, A. P., R. G. Jeffrey and E. Detournay (2005) Application of Scaling Laws to Laboratory-Scale Hydraulic Fractures. *Proc 40th North American Rock Mechanics Symposium*. Anchorage. Paper No. 818.
4. Casas, L. A., J. L. Miskimins, A. D. Black and S. J. Green (2006). Laboratory Hydraulic Fracturing Test on a Rock With Artificial Discontinuities. *Society of Petroleum Engineers.*
5. Cheng, W., Y. Jin and M. Chen (2015) Experimental study of step-displacement hydraulic fracturing on naturally fractured shale outcrops. *J. Geophys. Eng.* (12) 4:714-723.
6. Grosse, C. U. and M. Ohtsu (2008). Acoustic Emission Testing*. Springer.*
7. Haimson, B., and C. Fairhurst (1969). Hydraulic Fracturing in Porous-Permeable Materials. *Society of Petroleum Engineers*. (21) 7: 811-817
8. Ishida T, Q. Chen, Y. Mizuta and J. Roegiers (2014) Influence of Fluid Viscosity on the Hydraulic Fracturing Mechanism. ASME *J. Energy Resour. Technol.* 126(3):190-200
9. Lecampion, B., J. Desroches, R. G. Jeffrey, A. P. Bunger and J. Burghardt (2015). Initiation Versus Breakdown Pressure of Transverse Radial Hydraulic Fracture: Theory and Experiments. *ISRM 13th International Congress of Rock Mechanics.* Montreal
10. Morgan, S. P. and H. H. Einstein (2014). The Effect of Bedding Plane Orientation on Crack Propagation and Coalescence in Shale. *Proc 48th North American Rock Mechanics Symposium*. Minneapolis. Paper No. 7727.
11. Shearer, P. M. (2009). Introduction to Seismology. Cambridge University Press.
12. Solberg, P., D. Lockner and J. D. Byerlee (1980) Hydraulic Fracturing Granite under geothermal conditions. *Int. J. Rock Mech. Min. Sci. & Geomech. Abstr. (17) 1:25-33.*
13. Stanchitis, S., J. Burghardt and A. Surdi (2015) Hydraulic fracturing of heterogeneous rock monitored by acoustic emission. *Rock Mech Rock Eng*. 48: 2513.
14. Stanchitis, S., J. Desroches, J. Burghardt, A. Surdi and N. Whitney (2015) Rock Fabric Influence on Hydraulic Fracture. *Proceedings of 77th EAGE Conference and Exhibition.* Madrid.
15. Stoeckhert, F., S. Brenne, M. Molenda and M. Alber (2014). Fracture Mechanical Evaluation of Hydraulic Fracturing Laboratory Experiments. *ISRM - Rock Engineering and Rock Mechanics: Structures in and on Rock Masses.* Taylor & Francis Group*,* London. 1335-1340.
16. Zeng, Z., and J. C. Roegiers (2002). Experimental Observation of Injection Rate Influence on the Hydraulic Fracturing Behavior of a Tight Gas Sandstone. Society of Petroleum Engineers. *SPE/ISRM Rock Mechanics Conference.* Irvine, Texas. Paper No. 78172
17. Zoback, M.D., F. Rummel, R. Jung and C. B. Raleight (1977) Laboratory Hydraulic fracturing experiments in intact and pre-fractured rock. *Int. J. Rock Mech. Min. Sci. & Geomech. Abstr.* 14:49-58.